arXiv:cond-mat/0305211v1 9 May 2003

Equilibrium phase behavior of polydisperse hard spheres

Moreno Fasolo* and Peter Sollich†
Department of Mathematics, King's College London, London WC2R 2LS, U.K.
(Dated: January 10, 2022)

We calculate the phase behavior of hard spheres with size polydispersity, using accurate free energy expressions for the fluid and solid phases. Cloud and shadow curves, which determine the onset of phase coexistence, are found exactly by the moment free energy method, but we also compute the complete phase diagram, taking full account of fractionation effects. In contrast to earlier, simplified treatments we find no point of equal concentration between fluid and solid or re-entrant melting at higher densities. Rather, the fluid cloud curve continues to the largest polydispersity that we study (14%); from the equilibrium phase behavior a terminal polydispersity can thus only be defined for the solid, where we find it to be around 7%. At sufficiently large polydispersity, fractionation into several solid phases can occur, consistent with previous approximate calculations; we find in addition that coexistence of several solids with a fluid phase is also possible.

PACS numbers: 82.70.Dd, 64.10.+h, 82.70.-y, 05.20.-y

During the past few decades, a great deal of effort has been devoted to studies of the phase behavior of spherical particles, and in particular of the freezing transition, where the particles arrange themselves into a crystal with long-range translational order. The simplest system for studying this transition is one where the particles act as hard spheres, exhibiting no interaction except for an infinite repulsion on overlap. This scenario can be realized experimentally, using e.g., colloidal latex particles sterically stabilized by a polymer coating [1]. Hard spheres constitute a purely entropic system; the internal energy U vanishes, and $F = -TS$. Phase transitions are thus entropically driven; nevertheless, monodisperse (i.e., identically sized) hard spheres exhibit a freezing transition, where a fluid with a volume fraction of $\phi \approx 50\%$ coexists with a crystalline solid with $\phi \approx 55\%$ [2].

For colloidal hard spheres, there is inevitably a spread in the particle diameters σ, which are effectively continuously distributed within some interval. The width of the diameter distribution can be characterized by a polydispersity parameter δ, defined as the standard deviation of the size distribution divided by its mean.

The effect of polydispersity on the phase behavior of hard spheres has been investigated by experiments [1, 2], computer simulations [3, 4, 5, 6], density functional theories [7, 8], and simplified analytical theories [6, 9, 10, 11, 12, 13, 14]; Ref. [6] has a more detailed bibliography of earlier work. These studies have revealed that, compared to the monodisperse case, polydispersity causes several qualitatively new phenomena. First, it is intuitively clear [9] that significant diameter polydispersity should destabilize the crystal phase, because it is difficult to accommodate a range of diameters in a lattice structure. Experiments indeed show that crystallization is suppressed above a *terminal polydispersity* of $\delta_t \approx 12\%$ [1, 2]. Theoretical work suggested that this arises from a progressive narrowing of the fluid-solid coexistence region with increasing δ, with the phase boundaries meeting at δ_t [8, 10] in a point of equal concentration [13]. Bartlett and Warren [13] also found *re-entrant melting* on the high-density side of this point: for δ just below δ_t, they predicted that compressing a crystal could transform it back into a fluid, as sketched in the inset of Fig. 1 below. However, none of these theoretical studies fully accounted for *fractionation* [15], i.e., the fact that coexisting phases generally have different diameter distributions; in fluid-solid coexistence, one typically finds that the solid contains a higher proportion of the larger particles. Beyond the resulting difference in mean diameter, fractionation implies that coexisting phases can also have different polydispersities δ. Indeed, numerical simulations that allow for fractionation show that a solid with a narrow size distribution can coexist with an essentially arbitrarily polydisperse fluid [5, 16], suggesting that the concept of a terminal polydispersity is useful only for the solid but not for the fluid. Fractionation has also been predicted to lead to *solid-solid coexistence* [11, 12], where a broad diameter distribution is split into a number of narrower solid fractions. This occurs because the loss of entropy of mixing is outweighed by the better packing, and therefore higher entropy, of crystals with narrow size distribution; accordingly, as the overall polydispersity of the system grows, the number of coexisting solids is predicted to increase.

Previous work as described above leaves open a number of questions. The drastic and differing approximations for size fractionation used in the studies of reentrant melting and solid-solid coexistence [11, 12, 13] leave the relative importance of these two phenomena unclear. In [13] fractionation was allowed, but coexisting phases were implicitly constrained to have the same δ; calculations that account fully for fractionation remain restricted to highly simplified van der Waals free energies [14]. Numerical simulations have been carried out at constant chemical potential distribution [4, 16]; in con-

*Electronic address: moreno.fasolo@kcl.ac.uk
†Electronic address: peter.sollich@kcl.ac.uk

trast to the experimental situation, the overall particle size distribution can then change dramatically across the phase diagram, limiting the applicability of the results.

Our goal in this letter is to calculate the equilibrium phase behavior of polydisperse hard spheres on the basis of accurate free energy expressions, taking full account of fractionation and going beyond previous work on fluid-solid and solid-solid coexistence. The experimentally observed behavior of hard sphere colloids will of course also depend on non-equilibrium effects, e.g., the presence of a kinetic glass transition [17], anomalously large nucleation barriers [18] or the growth kinetics of polydisperse crystals [19]. Nevertheless, the equilibrium phase behavior needs to be understood as a baseline from which non-equilibrium effects can be properly attributed. Also, more of the equilibrium behavior may be observable under microgravity conditions, where the glass transition is shifted to higher densities or even absent [20].

Our calculations will show that the fluid cloud curve, which locates the onset of phase coexistence coming from low density, continues to large polydispersities δ: the point of equal concentration found in [13] disappears together with the predicted re-entrant melting. Instead of returning to a single-phase fluid at high volume fractions, the system splits into two or more fractionated solids, consistent with the simplified calculations of [11]; coexistence of several solids with a fluid phase appears as a new feature.

In general, the total free energy (density) of a polydisperse system consists of an ideal and an excess part ($f_{\rm ex}$). In units where $k_{\rm B}T = 1$,

$$f = \int d\sigma \rho(\sigma)[\ln \rho(\sigma) - 1] + f_{\rm ex} \qquad (1)$$

Here $\rho(\sigma)$ is the density distribution, i.e., $\rho(\sigma)\, d\sigma$ is the number density of particles with diameters between σ and $\sigma + d\sigma$. Equilibrium requires equality of the chemical potentials $\mu(\sigma) = \delta f/\delta\rho(\sigma)$ and of the pressure $\Pi = -f + \int d\sigma \mu(\sigma)\rho(\sigma)$ among all coexisting phases $a = 1 \ldots P$. Particle conservation adds the condition that, if phase a occupies a fraction $v^{(a)}$ of the system volume, then $\sum_a v^{(a)}\rho^{(a)}(\sigma) = \rho^{(0)}(\sigma)$, where $\rho^{(0)}(\sigma)$ is the overall or "parent" density distribution.

For the *fluid*, the most accurate free energy approximation available at present is the BMCSL generalization [21, 22] of the monodisperse Carnahan-Starling equation of state. This is *truncatable* in the sense that the excess free energy only depends on the four *moments* $\rho_i = \int d\sigma\, \sigma^i \rho(\sigma)$ $(i = 0 \ldots 3)$ of the density distribution [23]; ρ_0 is the total number density, $(\pi/6)\rho_3 = \phi$ the volume fraction, and $\rho_1/\rho_0 = \bar{\sigma}$ and $\rho_2/\rho_0 = \overline{\sigma^2}$ give the mean and mean-square diameter. For the crystalline *solid*, Bartlett [10, 24] assumed that the same truncatable structure holds; an approximate excess free energy (depending only on the same ρ_i) can then be derived from simulation results [25] for bidisperse hard spheres. Implicit in the use of data from [25] is the assumption that the crystal has a substitutionally disordered f.c.c. structure.

We adopt the BMCSL and Bartlett free energies for our calculation; the appropriate branch for a given $\rho(\sigma)$ is selected by taking the minimum of the fluid and solid free energies. Since the excess free energies depend only on the ρ_i, the excess chemical potentials $\mu_{\rm ex}(\sigma)$ take the form

$$\mu_{\rm ex}(\sigma) = \delta f_{\rm ex}/\delta\rho(\sigma) = \mu_0 + \mu_1\sigma + \mu_2\sigma^2 + \mu_3\sigma^3 \qquad (2)$$

For the solid, Bartlett [24] derived μ_0 and μ_3 from the small and large σ limits of the Widom insertion principle [26]. However, because of the approximate character of the excess free energy, $\mu_{\rm ex}(\sigma)$ then does not obey the thermodynamic consistency requirement $\delta\mu_{\rm ex}(\sigma)/\delta\rho(\sigma') = \delta\mu_{\rm ex}(\sigma')/\delta\rho(\sigma)$. To avoid this, we assign all excess chemical potentials by explicitly carrying out the differentiation in (2).

Our computational approach is based on the moment free energy method [27, 28, 29], which maps the full free energy (1), with its dependence on all details of $\rho(\sigma)$ through the ideal part, onto a moment free energy depending only on the moments ρ_i. For truncatable free energies this locates exactly the cloud points, i.e., the onset of phase separation coming from either a single-phase fluid or solid, as well as the properties of the coexisting "shadow" phases that appear there. Inside the coexistence region, one in principle needs to solve a set of highly coupled nonlinear equations [15] and the moment free energy method gives only approximate results. However, by retaining extra moments with adaptively chosen weight functions [29, 30, 31], increasingly accurate solutions can be obtained by iteration. Using these as initial points, we are then able to find full solutions of the exact phase equilibrium equations. Care is taken to check that solutions are globally stable, i.e., that no phase split of lower free energy exists [29]. We are able to calculate coexistence of up to $P = 5$ phases, which so far has been possible only for much simpler free energies depending on a single density moment (see e.g., [29]).

Below we present results for a symmetric triangular parent density distribution, i.e., $\rho^{(0)}(\sigma)$ increasing linearly from zero for $\sigma \in [1 - w, 1]$ and decreasing linearly for $\sigma \in [1, 1 + w]$, with $w = \sqrt{6}\delta$. The mean diameter of 1 fixes our length unit. Other distributions could be considered, but for the moderate values of δ of interest here one expects them to give qualitatively similar results, based on the intuition that for narrow size distributions δ is the key parameter controlling the phase behavior [9].

Fig. 1 shows our results for the cloud and shadow curves. The fluid cloud curve continues throughout the whole range of polydispersities that we can investigate: even at $\delta = 14\%$, a hard sphere fluid will eventually split off a solid on compression. Fractionation is key here; as indicated in Fig. 1, the coexisting shadow solid always has a smaller polydispersity, with δ never rising above 6%. This fractionation effect prevents the convergence of

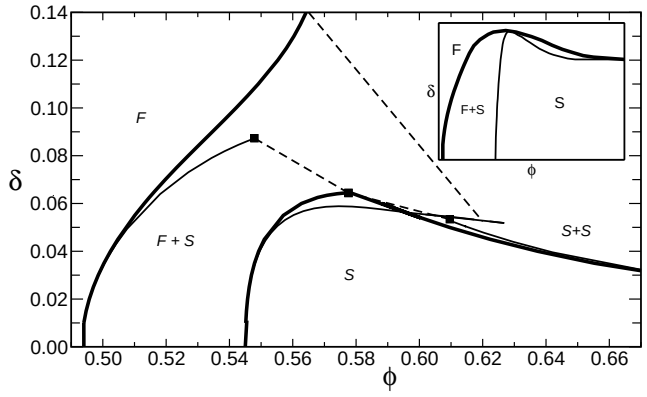


FIG. 1: Cloud (thick) and shadow (thin) curves, plotted as polydispersity δ versus volume fraction ϕ; dashed lines link sample cloud-shadow pairs. The fluid (F) cloud curve continues up to the largest δ that we study. The solid (S) cloud curve has two branches, with onset of F-S and S-S coexistence at low and high volume fractions, respectively. Inset: Sketch of the phase diagram of [13], showing re-entrant melting and the point of equal concentration.

the solid and fluid phase boundaries, along with the resulting re-entrant melting [13] (Fig. 1-inset). These findings are in qualitative accord with numerical simulations for the simpler case of fixed chemical potentials [5, 16]. In particular, the terminal polydispersity δ_t cannot be defined as the point beyond which a fluid at equilibrium will no longer phase separate; δ_t only makes sense as the maximum polydispersity at which a single solid phase can exist. As in [5] we also find that the coexisting fluid always has a lower volume fraction than the solid, along with (not shown) a lower mean diameter.

Coming from the single-phase solid, decreasing density at low polydispersities leads to conventional fluid-solid phase separation. At higher δ, however, the solid cloud curve acquires a second branch at higher densities. This is broadly analogous to the re-entrant phase boundary found in [13], but with the crucial difference that the system phase separates into two solids rather than a solid and a fluid. The two branches meet at a triple point. Here the solid cloud phase coexists with two shadow phases, one fluid and one solid, as marked by the squares in Fig. 1. From Fig. 1 the triple point, at $\delta_t \approx 7\%$, also gives the terminal polydispersity beyond which solids with triangular diameter distribution are unstable against phase separation. As explained, other distributions should give similar values of δ_t.

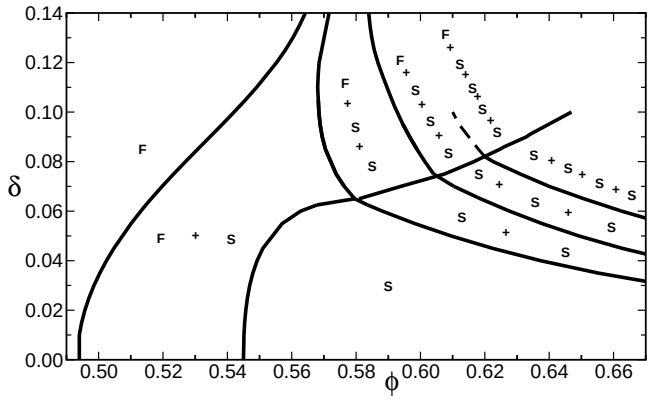


FIG. 2: Full phase diagram for polydisperse hard spheres with a triangular size distribution. In each region the nature of the phase(s) coexisting at equilibrium is indicated (F: fluid, S: solid). Dashed line: best guess for the phase boundary in the region where our numerical data become unreliable.

In Fig. 2 we show the full phase diagram for our triangular parent distribution. In each region the nature of the phase(s) coexisting at equilibrium is indicated. The cloud curves of Fig. 1 reappear as the boundaries between single-phase regions and areas of fluid-solid or solid-solid coexistence. Starting from the latter and increasing density or δ, fractionation into multiple solids occurs. The overall shape of the phase boundaries in this region is in good qualitative agreement with the approximate calculations of [11]. However, the coexisting solids do not necessarily split the diameter range evenly among themselves as assumed in [11]; see the sample plot in Fig. 3 of the normalized diameter distributions $n(\sigma) = \rho(\sigma)/\rho_0$ of four coexisting solids. In fact, plotting δ vs ϕ for all coexisting solids across the phase diagram, we find points that cluster very closely around the high-density branch of the solid cloud curve in Fig. 1. Coexisting solids with lower volume fraction ϕ thus tend to have higher polydispersity δ, as in the example in Fig. 3; this conclusion is intuitively appealing since higher compression should disfavor a polydisperse crystalline packing.

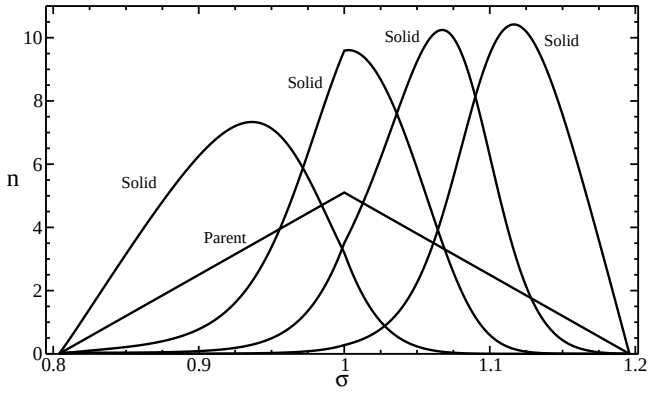


FIG. 3: Normalized diameter distribution of four coexisting solid phases obtained from a parent with $(\phi, \delta) = (63.0\%, 8\%)$. From left to right, the solids have volume fractions and polydispersities $(60.1\%, 5.4\%)$, $(62.9\%, 4.6\%)$, $(64.6\%, 4.0\%)$, $(66.3\%, 3.6\%)$.

Note that in Fig. 2, at larger δ than we can tackle numerically, coexistence of $P > 4$ solids would be expected since each individual solid can only tolerate a finite amount of polydispersity. However, from Fig. 2 such phase splits would occur at increasing densities and eventually be limited by the physical maximum volume

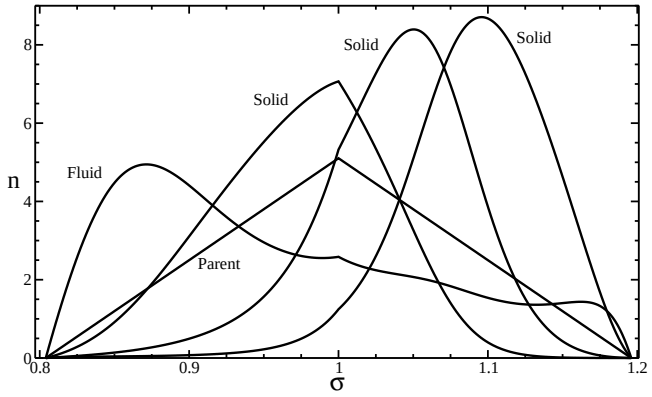


FIG. 4: Normalized diameter distributions for F-S-S-S phase coexistence obtained from a parent with $(\phi, \delta) = (60.3\%, 8\%)$.

fraction $\phi_{\max} \approx 74\%$. Also, at higher δ more complicated single-phase crystal structures, with different lattice sites occupied preferentially by (say) smaller and larger spheres, could appear and compete with the substitutionally disordered solids we consider.

Finally, a new feature of the phase diagram in Fig. 2 is the coexistence of a fluid with multiple solids. The triple point on the solid cloud curves already indicated the existence of a three-phase F-S-S region; as in the case of solid-solid phase splits, more solid phases then appear with increasing δ. Fig. 4 shows again that the fractionation behavior is non-trivial: while the coexisting fluid is enriched in the smaller particles as expected, it also contains "left over" large spheres that did not fit comfortably into the solid phases and thus ends up having a *larger* polydispersity (10.4%) than the parent (8%).

In conclusion, we have calculated the phase behavior of polydisperse hard spheres, using accurate free energies for the fluid and solid phases and solving exactly the resulting equilibrium conditions. Fluid-solid coexistence has been identified for fluids with polydispersities up to $\delta = 14\%$. This shows clearly that the experimentally observed suppression of crystallization above $\delta = 12\%$ is a non-equilibrium effect, probably caused by increased nucleation barriers at large δ [18]. For the solid, a terminal polydispersity remains well-defined as the maximal value beyond which instability to phase separation sets in; for triangular diameter distributions this turns out to be $\delta_t \approx 7\%$. Instead of the re-entrant melting predicted in an approximate treatment of fractionation effects [13], we find that sufficiently polydisperse solids split into two fractionated solids on compression. At higher volume fractions and polydispersities, multiple solids can coexist; coexistence of a fluid with several solids appears as a new feature. Fractionation effects are nontrivial, with solids splitting the diameter range unevenly among them and coexisting fluids sometimes having larger polydispersities than the parent.

Overall, our calculated phase diagram unites, clarifies and extends the previous separate predictions of polydispersity effects on fluid-solid coexistence and solid-solid fractionation. Numerical simulations may offer the best avenue for testing our predictions but will need to be carried out at fixed parent size distribution [32] to detect the complex fractionation phenomena we find. For the future it would be exciting to unify our predictions with those for fluid-fluid demixing, but this will be very challenging since the latter only occurs at polydispersities δ of order 100% [33, 34], far outside the range studied here.

It is a pleasure to thank Paul Bartlett for providing his code for the solid free energy. Financial support through EPSRC grant GR/R52121/01 is acknowledged.

[1] P. N. Pusey and W. van Megen, Nature **320**, 340 (1986).
[2] P. N. Pusey, in *Liquids, freezing and glass transition*, edited by J. P. Hansen, D. Levesque, and J. Zinn-Justin (North-Holland, Amsterdam, 1991).
[3] E. Dickinson and R. Parker, J. Phys. Lett. **46**, L229 (1985).
[4] P. G. Bolhuis and D. A. Kofke, Phys. Rev. E **54**, 634 (1996).
[5] P. G. Bolhuis and D. A. Kofke, J. Phys. Cond. Matt. **8**, 9627 (1996).
[6] S. E. Phan, W. B. Russel, J. X. Zhu, and P. M. Chaikin, J. Chem. Phys. **108**, 9789 (1998).
[7] J. L. Barrat and J. P. Hansen, J. Phys. (Paris) **47**, 1547 (1986).
[8] R. McRae and A. D. J. Haymet, J. Chem. Phys. **88**, 1114 (1988).
[9] P. N. Pusey, J. Phys. (Paris) **48**, 709 (1987).
[10] P. Bartlett, J. Chem. Phys. **107**, 188 (1997).
[11] P. Bartlett, J. Chem. Phys. **109**, 10970 (1998).
[12] R. P. Sear, Europhys. Lett. **44**, 531 (1998).
[13] P. Bartlett and P. B. Warren, Phys. Rev. Lett. **82**, 1979 (1999).
[14] H. Xu and M. Baus, J. Chem. Phys. **118**, 5045 (2003).
[15] P. Sollich, J. Phys. Cond. Matt. **14**, R79 (2002).
[16] D. A. Kofke and P. G. Bolhuis, Phys. Rev. E **59**, 618 (1999).
[17] P. N. Pusey and W. van Megen, Phys. Rev. Lett. **59**, 2083 (1987).
[18] S. Auer and D. Frenkel, Nature **413**, 711 (2001).
[19] R. M. L. Evans and C. B. Holmes, Phys. Rev. E **64**, 011404 (2001).
[20] J. X. Zhu *et al.*, Nature **387**, 883 (1997).
[21] T. Boublik, J. Chem. Phys. **53**, 471 (1970).
[22] G. A. Mansoori, N. F. Carnahan, K. E. Starling, and T. W. Leland, Jr., J. Chem. Phys. **54**, 1523 (1971).
[23] J. J. Salacuse and G. Stell, J. Chem. Phys. **77**, 3714 (1982).
[24] P. Bartlett, Mol. Phys. **97**, 685 (1999).
[25] W. G. T. Kranendonk and D. Frenkel, Mol. Phys. **72**, 679 (1991).
[26] B. Widom, J. Chem. Phys. **39**, 2808 (1963).
[27] P. Sollich and M. E. Cates, Phys. Rev. Lett. **80**, 1365

(1998).
[28] P. B. Warren, Phys. Rev. Lett. **80**, 1369 (1998).
[29] P. Sollich, P. B. Warren, and M. E. Cates, Adv. Chem. Phys. **116**, 265 (2001).
[30] N. Clarke *et al.*, J. Chem. Phys. **113**, 5817 (2000).
[31] A. Speranza and P. Sollich, J. Chem. Phys. **118**, 5213 (2003).
[32] N. B. Wilding and P. Sollich, J. Chem. Phys. **116**, 7116 (2002).
[33] P. B. Warren, Europhys. Lett. **46**, 295 (1999).
[34] J. A. Cuesta, Europhys. Lett. **46**, 197 (1999).